JMEPEG (2005) 14:136-143
DOI: 10.1361/10599490522257

1059-9495/$19.00

Multidisciplinary Optimization of Gas-Quenching Process

Zhichao Li and Ramana V. Grandhi

(Submitted January 28, 2002; in revised form March 2, 2004)

Distortion as a result of the quenching process is predominantly due to the thermal gradient and phase transformations within the component. Compared with traditional liquid quenching, the thermal boundary conditions during gas quenching are relatively simple to control. By adjusting the gas-quenching furnace pressure, the flow speed, or the spray nozzle configuration, the heat-transfer coefficients can be designed in terms of both the component geometry and the quenching time. The purpose of this research is to apply the optimization methodology to design the gas-quenching process. The design objective is to minimize the distortion caused by quenching. Constraints on the average surface hardness, and its distribution and residual stress are imposed. The heat-transfer coefficients are used as design variables. DEFORM-HT is used to predict material response during quenching. The response surface method is used to obtain the analytical models of the objective function and constraints in terms of the design variables. Once the response surfaces of the objective and constraints are obtained, they are used to search for the optimum heat-transfer coefficients. This process is then used instead of the finite-element analysis. A one-gear blank case study is used to demonstrate the optimization scheme.

Keywords distortion, finite element method, optimization, quenching, residual stress, response surface method

1. Introduction

The quenching of steel components is used to improve their mechanical properties, such as strength, hardness, and fatigue life. However, the thermal gradient and phase transformations may cause cracking and serious distortion problems. In industry, it is becoming increasingly important to reduce the distortion caused by heat-treatment processes (Ref 1). The ideal situation is to control the cooling process by adjusting the heat-transfer boundary conditions to minimize the distortion, while satisfying hardness and residual stress requirements.

During quenching, the steel component is first heated above the austenitization temperature and is held at that temperature to allow completion of the phase transformation to austenite. Then the hot component is cooled down rapidly to obtain the required properties. According to the quenchant used, the quenching process can be classified as liquid quenching or gas quenching.

High-pressure gas quenching has developed rapidly in the past 10 years (Ref 2, 3). Gas quenching has the disadvantage of a lower cooling rate than liquid quenching. However, the cooling severity of gas quenching has been improved by the use of efficient quenching gases and high-pressure quenching furnace designs. A heat-transfer coefficient of 3.0 W/m^2K can be obtained by gas quenching, which has a cooling severity that is equivalent to oil quenching (Ref 4). Flexible control over the component cooling history can be obtained during the gas-quenching process by the design of the spray nozzle configuration and its arrangement. More and more steel parts are being quenched with gas in industry (Ref 5, 6).

Computer simulation of the quenching process by the finite element analysis (FEA) has been developed in the past two decades (Ref 7-9). The heat transfer, phase transformations, and deformation are considered together to predict the quenching results. Designing the quenching process based on the computer simulation significantly reduces the design cost. Also, the computer simulation makes it possible to apply optimization technology to the design of the quenching process. Ruan (Ref 10) presented an inverse design methodology to obtain a required strength with an optimal cooling condition for the continuous quenching of precipitation-hardenable alloys. The conjugate method is used to optimize the cooling boundary conditions. Röhl and Srivatsa (Ref 11) minimized the cooling rate deviation in a nickel (Ni)-base superalloy turbine-engine, disk-quenching process. The finite-difference method is used to calculate the sensitivity information. The heat-transfer coefficients were used as design variables in the articles mentioned above, and gas quenching was used instead of the traditional liquid quenching. The research on the optimization design of the quenching process is limited. One reason why optimization cannot be easily used in the design of the quenching process is that sensitivity information is not available in the quenching simulation packages. Also, quenching is a highly nonlinear process with phase transformations or precipitations. Therefore, the sensitivity obtained by the analytical calculations may not be reliable. In this article, an alternative optimization method, which does not use the sensitivity information, is applied to optimize the gas-quenching process.

The response surface method (RSM) was first developed by Box and Wilson (Ref 12) in the statistical research field during the 1950s. This method is now widely used in many fields, such as chemistry, biology, and manufacturing. The main advantage of the RSM is the ability to optimize without using the sensitivity information. One goal of this research is to apply the RSM effectively to optimize the gas-quenching process.

The heat-transfer coefficients are adjusted during gas

Zhickao Li and **Ramana V. Grandhi,** Department of Mechanical and Materials Engineering, Wright State University, Dayton, OH 45435. Contact e-mail: rgrandhi@cs.wright.edu.

quenching by the furnace pressure, fluid flow speed, and the spray nozzle design. Investigations have shown that the values of the heat-transfer coefficient have a significant influence on the quenching results. In previous studies, the heat-transfer coefficient was modeled using a step function (Ref 13) in terms of quenching time, and it also has been modeled as varying along the component surface (Ref 14). Minimum distortion was obtained by designing the heat-transfer coefficient schedule. The optimum heat-transfer coefficient schedule can be calculated by the inverse techniques, using the cooling history information at several internal points (Ref 15, 16). As a result, the optimized heat-transfer coefficient can be implemented by checking the cooling history at several internal component points. In this article, the heat-transfer coefficient is designed in terms of both the component geometry and quenching time. The purpose of the optimum process design is to minimize the distortion while satisfying the hardness and residual stress requirements.

2. Computational Model

The simulation of the quenching process includes three main parts: heat transfer, phase transformations, and deformation. The three parts are influenced by each other during quenching. The basic formulations used for the computer simulation are introduced in this section.

2.1 Heat Transfer

The heat transfer follows Fourier's formula, as shown in Eq 1:

$$\rho\, c \frac{\partial T}{\partial t} = K \frac{\partial^2 T}{\partial X^2} + L_i \dot{\xi}_i \qquad \text{(Eq 1)}$$

where ρ is the density, c is the heat capacity, K is the heat-conduction coefficient, L_i is the latent heat due to phase transformation of the ith phase, and $\dot{\xi}_i$ is the transformation rate of the ith phase. In the finite element (FE) matrix format, the heat-transfer equation is described in Eq 2:

$$[K]T + [C]\dot{T} = Q(T, F) \qquad \text{(Eq 2)}$$

where $[K]$ is the heat conduction matrix, $[C]$ is the heat capacity matrix, $Q(T, F)$ is the heat load, and F is the volume fraction of different phases.

During quenching, the heat load vector includes two main parts: (a) the heat flux between the component surface and the quenchant and (b) the latent heat due to phase transformations.

$$Q(T, f) = \int_s h(T - T_e) dS + \int_v \Delta F_i \Delta E_i dV \qquad \text{(Eq 3)}$$

where Q is the heat load, h is the overall heat-transfer coefficient, which combines the influences of convection and radiation on the surface of the component, T is the surface temperature of the component, T_e is the quenchant temperature, ΔF_i is the volume of the ith phase transformed, and ΔE_i is the latent heat generated by the unit volume transformation of the ith phase.

2.2 Phase-Transformation Models

Diffusive phase transformations are modeled using the Johnson-Mehl-Avrami equation (Ref 17), which is given in Eq 4:

$$\xi_a = 1 - \exp(-f_T(T) t^n) \qquad \text{(Eq 4)}$$

where ξ_a is the volume fraction of austenite transformed, $f_T(T)$ is a function of temperature T, t is the phase transformation time, and the exponential n is a constant. The constant n and the function $f_T(T)$ are estimated by isothermal phase transformation diagrams.

Martensitic transformation is assumed to be purely temperature-driven, and it is modeled by the Magee's equation (Ref 18), which is given in Eq 5:

$$\xi_M = 1 - \exp(\psi_1 T + \psi_2) \qquad \text{(Eq 5)}$$

where ξ_M is the volume fraction of martensite, and ψ_1 and ψ_2 are constants, and they are determined by the martensitic transformation starting and finishing temperatures.

2.3 Stress and Deformation Analysis

The strain during quenching includes several terms, as shown in Eq 6:

$$d\varepsilon = d\varepsilon^e + d\varepsilon^p + d\varepsilon^t + d\varepsilon^{tr} + d\varepsilon^{tp} \qquad \text{(Eq 6)}$$

where the superscripts e, p, t, tr, and tp represent entities for elastic, plastic, thermal, transformation-induced plastic, and phase transformation plastic strains, respectively. The strain caused by phase transformation includes two parts: the strain caused by pure volume change due to transformation and the strain caused by the existence of deviatoric stress during transformation. The former and latter parts are represented by tp and tr, respectively.

3. Optimization Using RSM

Figure 1 shows how the RSM is implemented for optimization in this article. A certain number of design points are selected inside the design space, and then the computer simulations at those points are performed to predict the quenching results. The most interesting quenching results include distortion, hardness distribution, and residual stress. Quadratic response surface models are used to describe the relations between the quenching results and the design variables, as shown in Eq 7:

$$\eta = b_0 + \sum_{i=1}^{n} b_i x_i + \sum_{i=1}^{n} \sum_{j=i}^{n} b_{ij} x_i x_j \qquad \text{(Eq 7)}$$

where η is the concerned quenching result, b_i and b_{ij} are co-

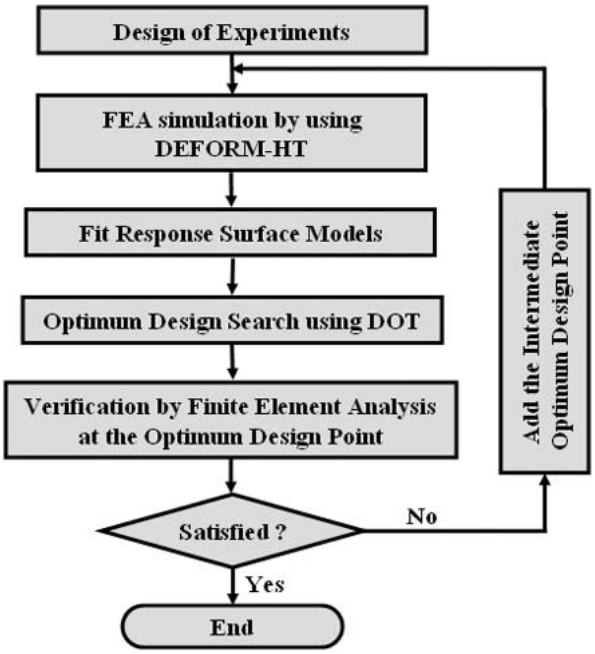

Fig. 1 Optimization procedure by RSM

efficients, x_i and x_j are the design variables, and n is the total number of design variables.

Using the least-squares method, as shown in Eq 8, the estimates of the regression coefficients are determined. The mixed regression method is used to improve the fitting accuracy of the response surface models by deleting some unimportant terms.

$$b = (X^T X)^{-1} X^T y \quad \text{(Eq 8)}$$

where b is the coefficient in Eq 7, X is the design variable vector, and y is the response vector of the objective function or constraints.

Once the closed-form equations, representing the relations between the quenching results and the design variables, are obtained, they are used to search for the optimum design instead of running further FEA simulations. The computational time spent on optimization is reduced significantly using this method. This is the main advantage of the RSM.

The response surfaces are approximate models of the FE simulations. Quenching is a highly nonlinear process. Therefore, the predicted quenching results obtained by the response surfaces may not match those obtained by FEA. To avoid this problem, the intermediate optimized quenching process provided by the response surfaces is added to the previous design of an experimental set. Then, the response surfaces are updated by adding the FE simulation results during the intermediate optimized quenching process. The iteration is continued until the optimization converges.

3.1 Gear Blank Case Study

The optimization methodology is demonstrated by an axisymmetric gear blank gas-quenching process design. The gear

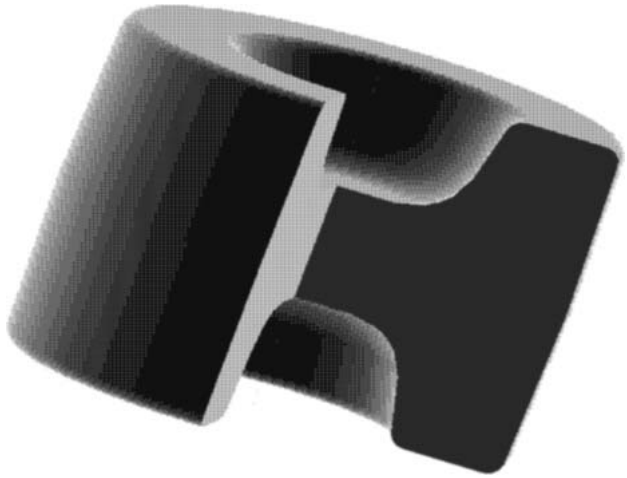

Fig. 2 Geometry of a gear blank

material is AISI 1050. The heat treating includes heating-up and cooling-down processes. In this article, only the cooling down by gas quenching is optimized. Before cooling, the gear blank is assumed to have a uniform temperature with pure austenite. The top and bottom of the gear blank are symmetric, as is shown in Fig. 2. Therefore, a quarter cross section is used for the simulation and optimization. The FE model includes 557 nodes and 505 elements, as shown in Fig. 3. The element side length is around 2 mm.

3.2 Optimization Model

The heat-transfer coefficients are considered to be the most important process parameters to affect quenching results. In this case study, the heat-transfer coefficients are used as design variables, and they are modeled in terms of both the component geometry and the quenching time. To pursue a more uniform cooling rate, different heat-flux rates should be imposed on concave and convex corners of the component. In this case study, the surface of the gear blank is divided into three regions, as shown in Fig. 4(a). At each region, a different heat-transfer coefficient schedule in terms of time is imposed.

Cubic splines are used to model the heat-transfer coefficients as a function of quenching time. The simulations of this gear blank model have shown that the heat-transfer coefficients have a significant effect on the quenching results during the first 100 s. As shown in Fig. 4(a), on each surface section three points are used to model the heat-transfer coefficient in terms of quenching time, which is shown in Fig. 4(b). The x-coordinates (quenching time) of all control points are fixed, and the y-coordinates of these control points are used as design variables to optimize the quenching process. Therefore, nine heat-transfer coefficient design variables are used to optimize the gas-quenching process.

The design space of this example is listed in Table 1. The values of heat-transfer coefficients imposed on the three divided surface regions at the middle of the design space are 2.0, 1.0, and 1.5 kW/m^{2}K, respectively. Two criteria are usually considered in the determination of the design space. The first is that the industry should have the ability to implement the de-

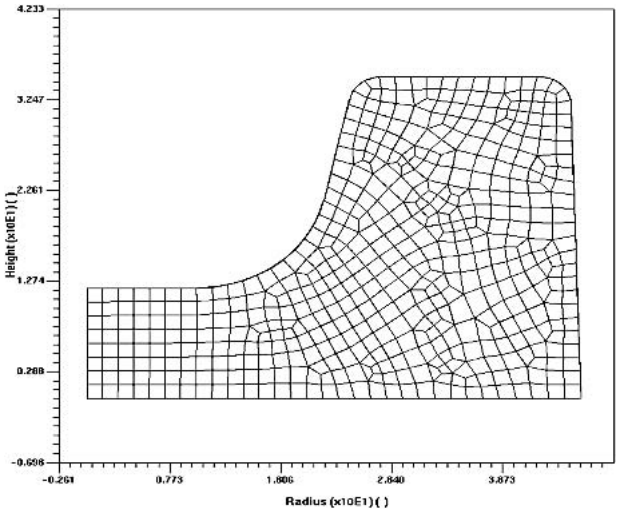

Fig. 3 Finite-element model

Table 1 Design space

Design variables	Lower bound, kW/m^{2}K	Middle point, kW/m^{2}K	Upper bound, kW/m^{2}K
$X(1)$	1.7	2.0	2.3
$X(2)$	1.7	2.0	2.3
$X(3)$	1.7	2.0	2.3
$X(4)$	0.7	1.0	1.3
$X(5)$	0.7	1.0	1.3
$X(6)$	0.7	1.0	1.3
$X(7)$	1.2	1.5	1.8
$X(8)$	1.2	1.5	1.8
$X(9)$	1.2	1.5	1.8

sign within the design space set. The second is that the optimum design point should be located inside the design space. Running several FEA simulations is usually helpful in determining the design space for a specified problem.

The objective of optimization is to minimize the distortion of the as-quenched gear blank. A schematic plot of the distortion definition used in this case study is shown in Fig. 5. The desired shape and the final shape are drawn as a solid line and a dotted line, respectively. The areas A, B, C, and D are the shape differences between the distorted and undistorted shapes. The distortion is defined as the addition of the absolute values of the four areas. According to different requirements, the distortion may have different definitions.

The standard deviation of the residual stress is used as the first constraint. The second and third constraints are imposed on the average surface hardness and its standard deviation.

Investigations on this case study have shown that the response surfaces of both the average surface hardness and its standard deviation have poor fitting accuracy. In this case study, the hardness values of three points located on the surface of the component are used to build the response surfaces. The three points are shown in Fig. 6. The average surface hardness and its standard deviation are calculated based on the hardness values at these three points. The average surface hardness is calculated by using Eq 9:

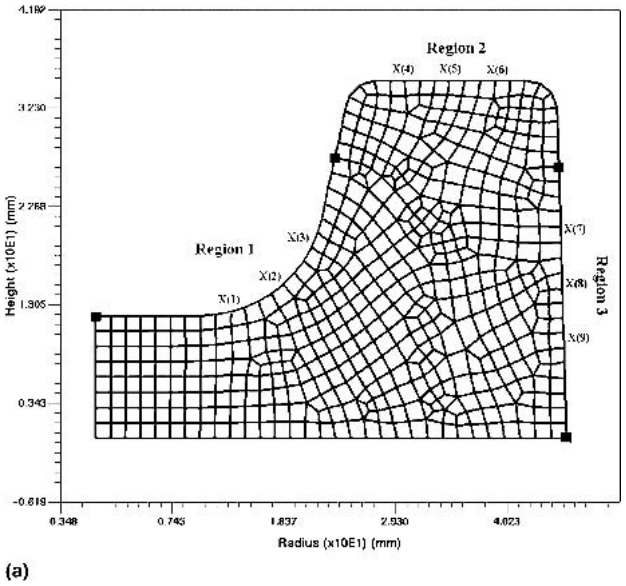

(a)

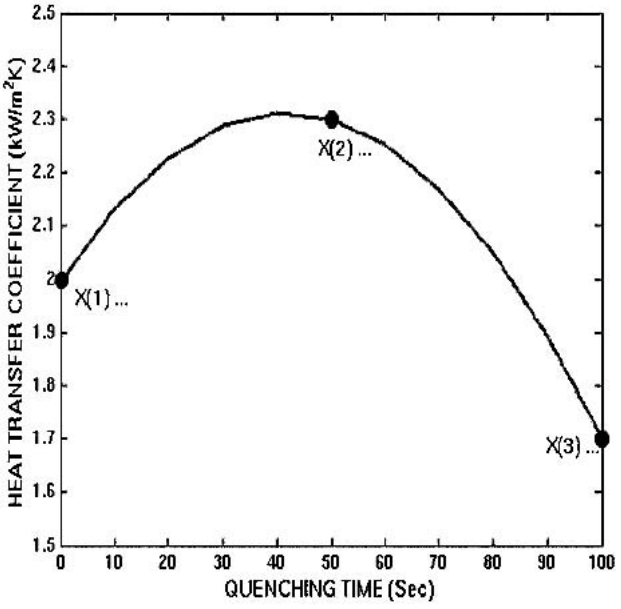

(b)

Fig. 4 Modeling of the heat-transfer coefficient in terms of (a) component geometry and (b) quenching time

$$\overline{H} = \frac{\sum_{i=1}^{3} H_i}{3} \quad \text{(Eq 9)}$$

where $\overline{H}$ is the average surface hardness of these three points. Variable H_i represents the hardness at the ith surface point.

The standard deviation of the surface hardness is calculated by Eq 10:

$$H_d = \sqrt{\frac{\sum_{i=1}^{3} (H_i - \overline{H})^2}{2}} \quad \text{(Eq 10)}$$

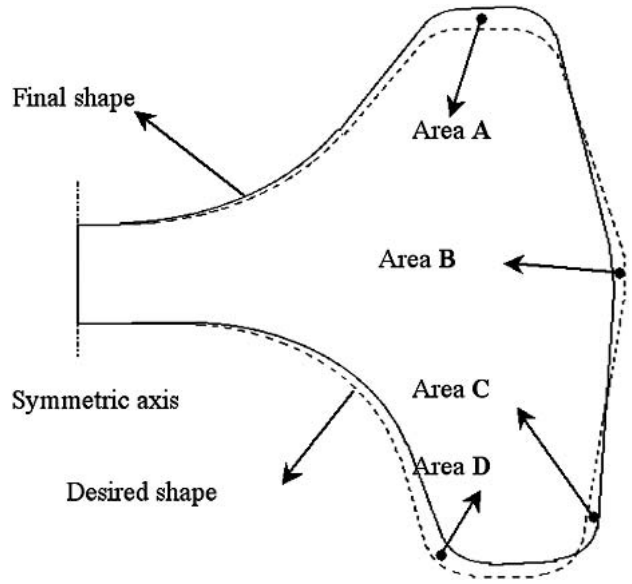

Fig. 5 Schematic plot of distortion

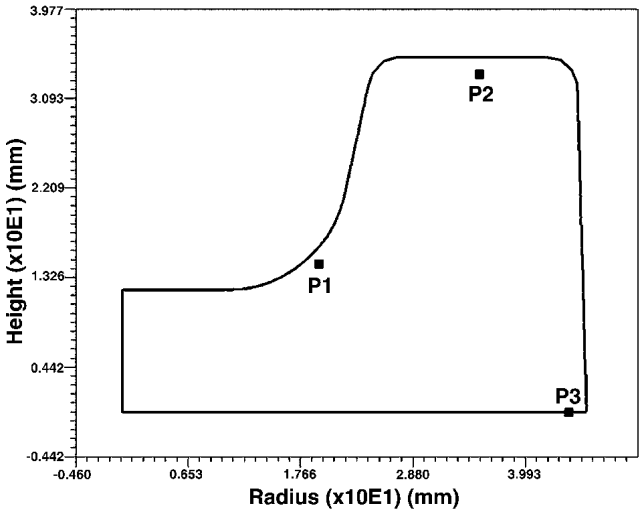

Fig. 6 Three control points on the surface of the component

where H_d is the standard deviation of the hardness based on the three surface points.

The optimization model shown below is in the standard normalized format.

Minimize:

$$\text{Obj} = \text{distortion}/1.0 \quad \text{(Eq 11)}$$

Subject to:

$$G(1) = \frac{\sigma_d}{350.0} - 1.0 \le 0 \quad \text{(Eq 12)}$$

$$G(2) = 1.0 - \frac{\overline{H}}{50.0} \le 0 \quad \text{(Eq 13)}$$

Table 2 Analysis of variance in distortion

Source of variation	Degrees of freedom	Sum of squares	Mean square	F ratio
Model	24	36.73	1.53	20.28
Error	87	6.56	0.075	
Total	111	43.29		

Table 3 Comparison of the optimum and reference designs

	Reference design	Optimum design
$X(1)$, (kW/m^{2}K)	1.5	2.19
$X(2)$, (kW/m^{2}K)	1.5	1.85
$X(3)$, (kW/m^{2}K)	1.5	1.72
$X(4)$, (kW/m^{2}K)	1.5	0.70
$X(5)$, (kW/m^{2}K)	1.5	0.96
$X(6)$, (kW/m^{2}K)	1.5	0.97
$X(7)$, (kW/m^{2}K)	1.5	1.35
$X(8)$, (kW/m^{2}K)	1.5	1.31
$X(9)$, (kW/m^{2}K)	1.5	1.20
Objective	3.99	1.52
$G(1)$	0.20	–0.010
$G(2)$	–0.030	–0.079
$G(3)$	9.12	–0.18
Distortion, mm^2	3.99	1.52
σ_d (MPa)	421.6	346.5
$\overline{H}$ (HRC)	51.49	53.97
H_d (HRC)	5.06	0.41

$$G(3) = \frac{H_d}{0.5} - 1.0 \le 0 \quad \text{(Eq 14)}$$

where σ_d is the standard deviation of the maximum principal residual stress, and $\overline{H}$ and H_d are the average surface hardness and its standard deviation, respectively.

Different methods can be used to design the experimental set for optimization. In this case study, D-optimality is used to design the experimental set. To build the response surface in terms of 9 design variables, 46 unknown parameters are included in the full quadratic polynomial models. A total of 90 design points are used to build the response surface models in this case study.

The mixed-regression method is used to delete some insignificant terms from the full quadratic polynomial to improve the fitting accuracy. A total of 22 iterations are performed before obtaining the satisfactory design. Table 2 is the analysis of variance of the distortion.

4. Results and Discussion

The optimized gas-quenching process design, together with a reference design, is shown in Table 3. In the reference design, a constant heat-transfer coefficient is imposed on the component surface. Also, the heat-transfer coefficient is independent of the quenching time. The optimum heat-transfer coefficients are shown in Fig. 7. The optimum design shows that two design variables, $X(4)$ and $X(9)$, are located at their lower bounds.

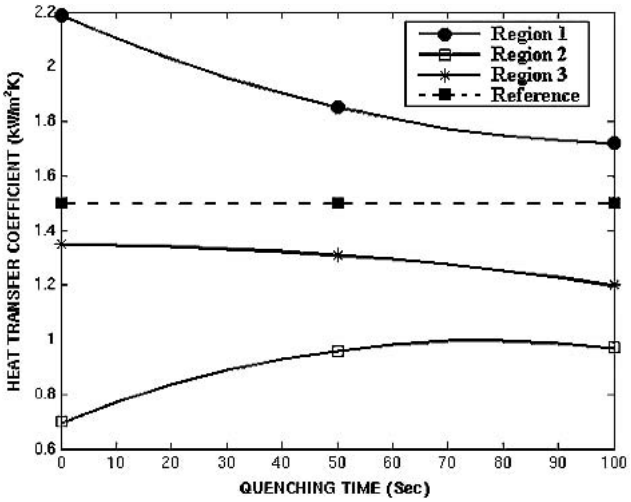

Fig. 7 Optimized schedule for heat-transfer coefficients

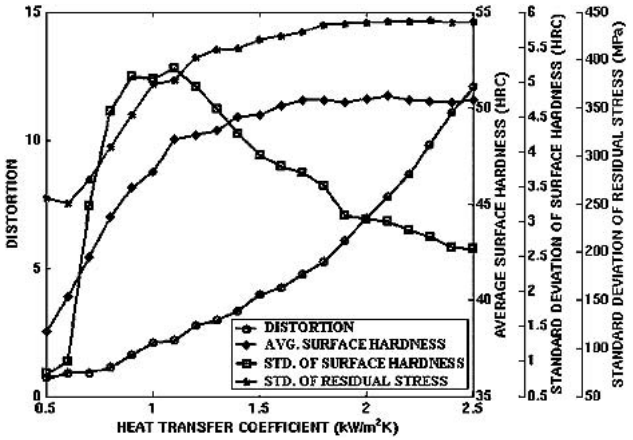

Fig. 8 Influences of the heat-transfer coefficient on the quenching results

From the optimization point of view, the objective function can be minimized further if the design space can be expanded. If the equipment available in industry can implement the gas-quenching process with the heat-transfer coefficient schedules of $X(4)$ (i.e., <0.7 kW/m^{2}K) and $X(9)$ (i.e., <1.2 kW/m^{2}K), the design space can be expanded by decreasing the lower bounds of $X(4)$ and $X(9)$. The iteration scheme shown in Fig. 1 can be continued within the expanded design space until convergence. In this case study, the design space was not expanded.

Comparing the optimum design with the reference design, the distortion is reduced from 3.99 to 1.52 mm^2. The standard deviation of the residual stresses is reduced from 421.6 to 346.5 MPa. Therefore, the constraint on the standard deviation of the residual stresses is satisfied. The constraint on the average surface hardness is satisfied for both the reference and optimum designs. After optimization, the constraints on both the average surface hardness and the standard deviation of the surface hardness are not active. The reason is shown schematically in Fig. 8. Figure 8 shows the effect of the heat-transfer coefficients on the quenching results. A constant heat-transfer coefficient is imposed on the surface of the component, and the heat-transfer coefficient is constant with time. As the heat-transfer coefficient increased, distortion increased. Therefore, to minimize the distortion in cases in which the constraints are not considered, the heat-transfer coefficient should take the least value. As the heat-transfer coefficient increases, both the standard deviation of the residual stress and the average surface hardness increase. To obtain enough surface hardness after quenching, high values of the heat-transfer coefficient are preferred. The standard deviation of the surface hardness increases with the increase of the heat-transfer coefficient first, and then it tends to decrease after the peak. The complexity between the quenching results and the heat-transfer coefficients shows that all the constraints do not have to be active after quenching. However, it is necessary to impose these constraints to optimize the gas-quenching process. Otherwise, the least heat-transfer coefficient value is always preferred, and the material cannot be hardened in this case. In Fig. 8, the heat-transfer coefficient is a constant in terms of both the component geometry and the quenching time. For a complex heat-transfer coefficient schedule, the relations between the quenching results and the design variables are more complex. However, Fig. 8 can still clearly explain why the constraints are not active.

Table 4 Comparison of RSM with FEM

Method	Distortion, mm^2	σ_d, MPa	$\overline{H}$, HRC	H_d
RSM	1.46	348.2	52.95	0.49
FEM	1.52	346.5	53.97	0.41
Absolute error	0.06	1.71	1.02	0.08
Relative error	3.95%	0.49%	1.89%	16.32%

The average surface hardness and its standard deviation are taken as two constraints to optimize the gas-quenching problem. After optimization, the surface hardness distribution is more uniform, compared with the reference design. Figure 9 shows the hardness distributions of both the reference design and the optimum design. A constant heat-transfer coefficient along the surface of the component is imposed in the reference design. The quenching results show that the hardness at the corner M is lower than the average surface hardness, as shown in Fig. 9(a). The hardness contour lines are discontinuous at the corner M. After optimization, the hardness contour lines are continuous along the component surface, which shows that the surface hardness distribution is more uniform. The contour magnitudes of both the reference and optimum hardness distributions show that their average surface hardness constraints are satisfied.

The standard deviation of the residual stress is used as a constraint to obtain a more uniform residual stress distribution. The residual stress contours of both the reference design and the optimum design are shown in Fig. 10. After optimization, the residual stress distribution is more uniform. A more uniform residual stress distribution after quenching is preferred to reduce the shape change during tempering or service.

At the optimum design point obtained by the response surface models, one FE simulation is performed to check the fitting accuracy of the response surface models. The comparison is shown in Table 4. The absolute and relative errors in the distortion, the standard deviation of the residual stress, and the

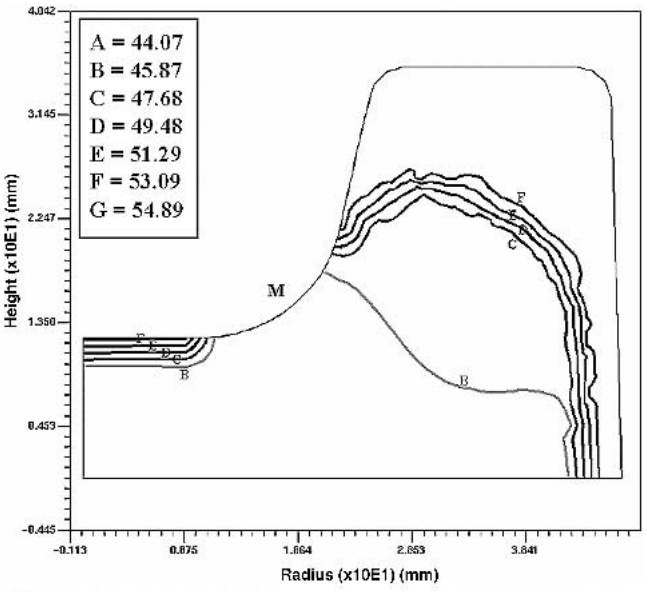

(a)

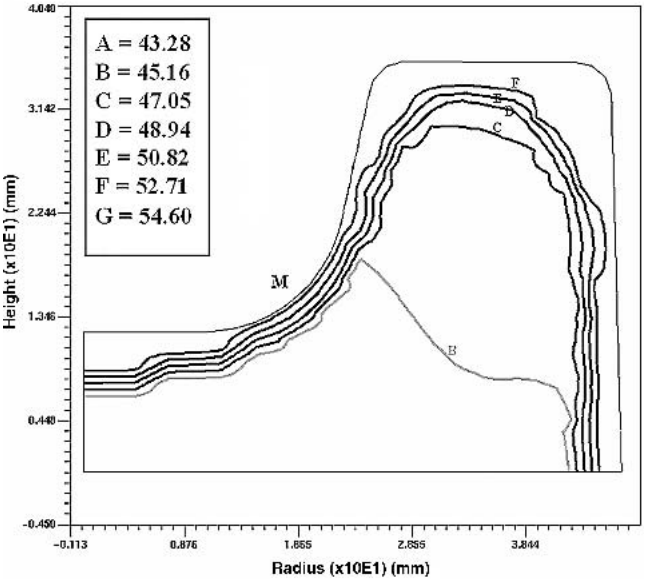

(b)

Fig. 9 Hardness distribution (HRC). (a) Reference design. (b) Optimum design

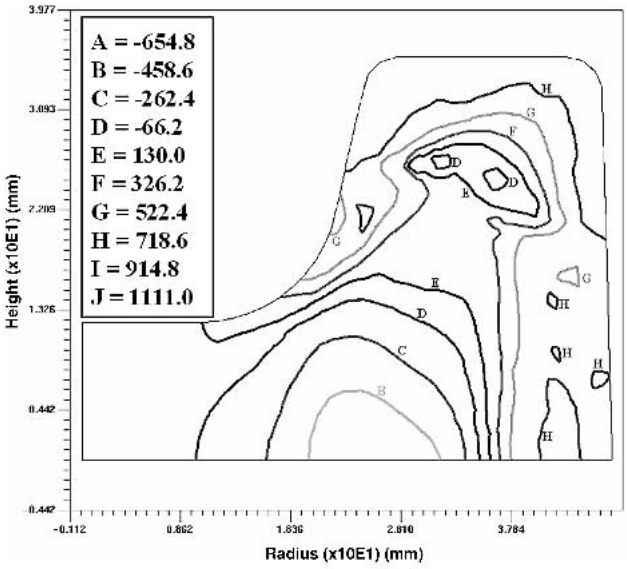

(a)

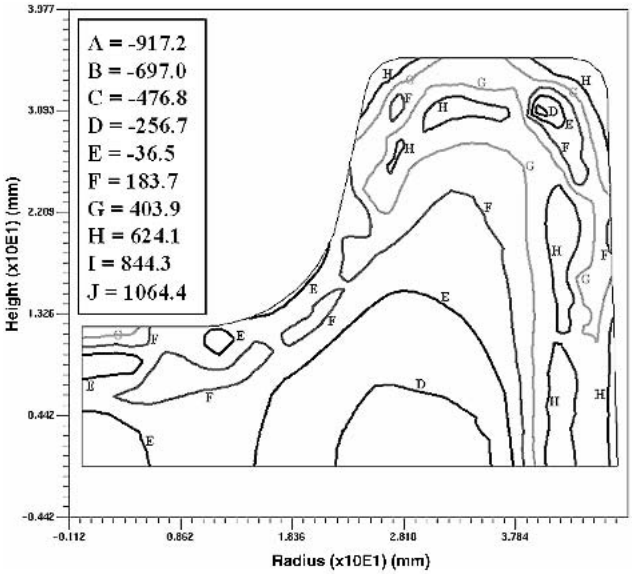

(b)

Fig. 10 Maximum principal stress distribution (megapascals). (a) Reference design. (b) Optimum design

average surface hardness are small. However, the relative error of the standard deviation of the surface hardness between RSM and FEA is as large as 16%. The reason for the large relative error is because the absolute value of the standard deviation of the surface hardness is small. Considering the reference design with the surface hardness standard deviation of 5.06, the response surface model of the surface hardness standard deviation is acceptable.

5. Conclusions

The heat-transfer coefficient is designed in terms of both the component geometry and the quenching time. This modeling of the heat-transfer coefficient can be implemented by designing a spray nozzle configuration and arrangement during gas quenching. The RSM provides an effective way to minimize the distortion, while satisfying the residual stress and surface hardness distribution requirements. The verification by the FE simulations shows that the optimum design point produced by the RSM improved the process without resorting to expensive trial and error procedures.

Acknowledgment

This project was funded by the National Institute of Standards and Technology, Advanced Technology Program, and Ohio State University Research Foundation no. 64921-55-00. The Graduate Research Assistantship for Dr. Li was supported by the Dayton Area Graduate Study Institute (DAGSI).

References

1. H. Altena, P. Stola, P. Jurci, F. Klima, and J. Paulu, Influence of Gas and Oil Quenching Parameters on Changes in Shape and Dimension of Gear Wheels, *Heat Treat. Met.,* Vol 1, 2001, p 1-8
2. K. Funatani, New Quenchants and Cooling Technology, Current Status and Future, *Third Int. Conf. Quenching and Control of Distortion* (Prague, the Czech Republic), ASM International, March 1999, p 5-16
3. S.J. Midea, T. Holm, S. Segerberg, J. Bodin, T. Thors, and K. Swärtstorm, High Pressure Gas Quenching: Technical and Economical Considerations, *Second Int. Conf. Quenching and the Control of Distortion* (Cleveland, OH), ASM International, Nov 1996, p 157-163
4. P. Heilmann, and W.R. Zenker, Gas Quenching Tool Steels, *Adv. Mater. Proc.,* Vol 2, 1993, p 29-31
5. G.C. Carter, Optimization Gas Quenching, *Adv. Mater. Proc.,* Vol 149 (No. 2), 1996, p 79-82
6. F.T. Hoffmann, T. Lübben, and P. Mayr, New Development in Quenching Systems and Equipment: Current Status and Future Developments, *Third Int. Conf. Quenching and Control of Distortion* (Prague, the Czech Republic), ASM International, March 1999, p 459-465
7. T.C. Tszeng, W.T. Wu, and J.P. Tang, Prediction of Distortion During Heat Treating and Machining Processes, *Proc. 16th ASM Heat Treating Society Conference and Exposition* (Cincinnati, OH), ASM International, 1996, p 9-15
8. T. Inoue and K. Arimoto, Development and Implementation of CAE System "HEARTS" for Heat Treatment Simulation Based on Metallo-Thermo-Mechanics, *J. Mater. Eng. Perf.,* Vol 6 (No. 1), 1997, p 51-60
9. B.L. Ferguson, A. Freborg, and G. Petrus, Software Simulates Quenching, *Adv. Mater. Proc.,* Vol 158 (No. 2), 2000, p 31-34
10. Y. Ruan, Inverse Optimal Design of Cooling Conditions for Continuous Quenching Processes, *Int. J. Numer. Methods Eng.,* Vol 51, 2001, p 127-142
11. P.J. Röhl and S.K. Srivatsa, "A Comprehensive Approach to Engine IPPD," AIAA report 97-1113, AIAA, 1997, p 1250-1257
12. G. Box and K. Wilson, On the Experimental Attainment of Optimum Condition, *J.R. Stat. Soc.,* Vol 13, 1951, p 1-45
13. Z. Li, G. Ramana, and R. Shivpuri, Optimum Design of Heat Transfer Coefficient During Gas Quenching Process by Using Response Surface Method, *J. Machine Tools Manufact.,* Vol 42, 2002, p 549-558
14. Z. Li, G. Ramana, and R. Srinivasan, Distortion Minimization During Gas Quenching Process, *J. Mater. Proc. Technol.* (in press)
15. B.H. Morales, J.K. Brimacombe, E.B. Hawbolt, and S.M. Gupta, Determination of Quench Heat-Transfer Coefficients Using Inverse Techniques, *First Int. Conf. Quenching and Control of Distortion* (Chicago, IL), ASM International, Sept 1992, p 155-164
16. S.G. Chen, C.I. Weng, and J. Lin, Inverse Estimation of Transient Temperature Distribution in the End Quenching Test, *J. Mater. Proc. Technol.,* Vol 86, 1999, p 257-263
17. W.A. Johnson and F.R. Mehl, Reaction Kinetics in Processes of Nucleation and Growth, *Trans. AIME*, Vol 135, 1939, p 416-425
18. C.L. Magee, "Phase Transformations," paper presented at Seminar of the American Society for Metals, ASM, 1968, p 115-154